Journal for ImmunoTherapy of Cancer

Inhibiting PLA2G7 reverses the immunosuppressive function of intratumoral macrophages and augments immunotherapy response in hepatocellular carcinoma

Feng Zhang,[1,2,3] Wenfeng Liu,[1,2,3] Fansheng Meng,[3] Qiuyu Jiang,[1,2,3] Wenqing Tang,[1,2,3] Zhiyong Liu,[1,2,3] Xiahui Lin,[1,2,3] Ruyi Xue,[1,2,3] Si Zhang,[3] Ling Dong [1,2,3]

To cite: Zhang F, Liu W, Meng F, *et al*. Inhibiting PLA2G7 reverses the immunosuppressive function of intratumoral macrophages and augments immunotherapy response in hepatocellular carcinoma. *Journal for ImmunoTherapy of Cancer* 2024;**12**:e008094. doi:10.1136/jitc-2023-008094

► Additional supplemental material is published online only. To view, please visit the journal online (http://dx.doi.org/10.1136/jitc-2023-008094).

FZ, WL and FM are joint first authors.

Accepted 11 December 2023

For numbered affiliations see end of article.

Correspondence to
Professor Ling Dong;
dong.ling@zs-hospital.sh.cn

Professor Si Zhang;
zhangsi@fudan.edu.cn

ABSTRACT

Background Hepatocellular carcinoma (HCC) is an exceptionally immunosuppressive malignancy characterized by limited treatment options and a dismal prognosis. Macrophages constitute the primary and heterogeneous immune cell population within the HCC microenvironment. Our objective is to identify distinct subsets of macrophages implicated in the progression of HCC and their resistance to immunotherapy.

Methods Intratumoral macrophage-specific marker genes were identified via single-cell RNA sequencing analyses. The clinical relevance of phospholipase A2 Group VII (PLA2G7), a pivotal enzyme in phospholipid metabolism, was assessed in patients with HCC through immunohistochemistry and immunofluorescence. Flow cytometry and an in vitro co-culture system were used to elucidate the specific role of PLA2G7 in macrophages. Orthotopic and subcutaneous HCC mouse models were employed to evaluate the potential of the PLA2G7 inhibitor in complementing immune checkpoint blockade (ICB) therapy.

Results Single-cell RNA sequencing analyses disclosed predominant PLA2G7 expression in intratumoral macrophages within the HCC microenvironment. The macrophage-specific PLA2G7 was significantly correlated with poorer prognosis and immunotherapy resistance in patients with HCC. PLA2G7^{high} macrophages represent a highly immunosuppressive subset and impede CD8 T-cell activation. Pharmacological inhibition of PLA2G7 by darapladib improved the therapeutic efficacy of anti-programmed cell death protein 1 antibodies in the HCC mouse models.

Conclusions Macrophage-specific PLA2G7 serves as a novel biomarker capable of prognosticating immunotherapy responsiveness and inhibiting PLA2G7 has the potential to enhance the efficacy of ICB therapy for HCC.

WHAT IS ALREADY KNOWN ON THIS TOPIC

⇒ Immune checkpoint inhibitors have shown limited efficacy in hepatocellular carcinoma (HCC). Targeting tumor-associated macrophages within the tumor microenvironment may provide promising strategies to potentiate therapy effectiveness.

WHAT THIS STUDY ADDS

⇒ Phospholipase A2 Group VII (PLA2G7) demonstrates predominant expression within intratumoral macrophages and exhibits associations with both prognosis and the response to immune checkpoint blockade in HCC. Macrophages characterized by elevated levels of PLA2G7 manifest a profoundly immunosuppressive phenotype, detrimentally impacting the activation of CD8 T cells. In vivo studies have substantiated that darapladib, an inhibitor of PLA2G7, enhances the susceptibility of HCC to anti-programmed cell death protein 1 therapy.

HOW THIS STUDY MIGHT AFFECT RESEARCH, PRACTICE OR POLICY

⇒ Our investigation has unveiled a previously unrecognized role of PLA2G7 as a biomarker and potential therapeutic target in HCC. This discovery introduces a promising strategy for combination therapy aimed at improving the management of immunotherapy in HCC.

BACKGROUND

Hepatocellular carcinoma (HCC) ranks as the sixth most prevalent malignancy and the third foremost contributor to cancer-related mortality worldwide, thereby constituting a pressing concern in the realm of public health.[1] Owing to the inconspicuous nature of symptoms during the initial stages, a majority of patients with HCC receive diagnoses at an advanced juncture, rendering curative surgical resection unviable.[2] Recently, immune checkpoint blockade (ICB), specifically inhibitors targeting programmed cell death protein 1 (PD-1),

has attracted significant attention within the domain of cancer therapy due to its potential to reinstate the antitumor immune response, thereby inducing enduring remissions.[3] However, due to the heterogeneity and pronounced invasiveness characteristic of HCC, the utilization of anti-PD-1 inhibitors as standalone interventions only yielded a meager objective response rate of 14% alongside a disease control rate of 56% among patients grappling with advanced HCC.[4 5] Therefore, the identification of proficient biomarkers capable of prognosticating the responsiveness to immune checkpoint inhibitors, in conjunction with the formulation of innovative targeted therapeutic agents designed to augment the effectiveness of ICB therapy, have arisen as central tenets within ongoing HCC research endeavors.

Macrophages, constituting the predominant immune cell population within the tumor microenvironment (TME), assume a dual role in the progression of HCC.[6] On the one hand, they possess the capability to promote antitumor responses by aiding in the recognition and elimination of tumor cells through antigen presentation and phagocytosis. Conversely, they can be re-educated into tumor-associated macrophages (TAMs) that functionally resemble alternative M2-like macrophages, thereby promoting disease progression.[7] TAM-derived immunosuppressive cytokines can hamper the function of cytotoxic T lymphocytes, fostering a profoundly immune-suppressed tumor environment that diminishes responsiveness to ICB therapy.[8] Nonetheless, TAMs exhibit notable plasticity, conferring on them the ability to embrace a wide spectrum of phenotypic, metabolic, and functional traits in retort to diverse local cues encountered within the confines of the TME. Thus, gaining a deeper understanding of the molecular landscapes that define TAMs within the HCC microenvironment and accurately identifying critical macrophage subsets are essential for reversing the immunosuppressive TME and complementing ICB therapy in HCC.

Phospholipase A2 Group VII (PLA2G7), also recognized as platelet-activating factor acetylhydrolase, is a member of the phospholipases A2 family, responsible for encoding the lipoprotein-associated phospholipase A2 (Lp-PLA2) protein. This enzyme plays a crucial role in catalyzing the hydrolysis of phospholipids, leading to the liberation of free fatty acids and lysophospholipids.[9] The significance of PLA2G7 has been firmly entrenched across a spectrum of metabolic and inflammatory disorders, encompassing conditions such as atherosclerosis,[10] diabetes,[11] and autoimmune diseases.[12] Recent investigations have also alluded to the potential of PLA2G7 to emerge as a promising biomarker, with diagnostic and prognostic implications, within diverse categories of malignancies.[13–16] Furthermore, it is proposed that PLA2G7 has the potential to directly regulate the proliferation and apoptosis of tumor cells.[15 17] Nonetheless, a dearth of exploration remains concerning the role of PLA2G7 within the immune microenvironment of malignancies. The plausible significance of PLA2G7 as a modulator of antitumor immunity, along with its implications for tailored cancer immunotherapy, necessitates deeper scrutiny.

In this study, through high-throughput single-cell analyses, we have demonstrated that PLA2G7 exhibits primary expression within intratumoral macrophages in the HCC microenvironment. Patients with HCC displaying elevated levels of both PLA2G7 and CD68 experienced the poorest survival outcomes and demonstrated reduced responsiveness to anti-PD-1 antibodies. Additionally, PLA2G7^{high} macrophages exhibited diminished potential for promoting pro-inflammation and supporting T-cell immunity when compared with PLA2G7^{low} macrophages. In vivo pharmacological inhibition of PLA2G7 with darapladib sensitized HCC to anti-PD-1 therapy. This study has revealed a previously unrecognized role for PLA2G7 as a potent adjunct target for enhancing the effectiveness of ICB therapy in HCC.

METHODS

Patients and specimens

For public database analysis, the RNA-sequencing and clinical data of The Cancer Genome Atlas liver hepatocellular carcinoma (TCGA-LIHC) cohort (374 patients) and the Gene Expression Omnibus (GEO) cohort with accession numbers GSE14520 (225 patients) were downloaded. The transcriptome data underwent normalization using the "limma" package in the R software before proceeding with subsequent analyses.

For HCC tissue microarray construction, we used 130 formalin-fixed, paraffin-embedded HCC tissues obtained from consecutive patients who underwent curative resection at the Liver Cancer Institute, Fudan University, Shanghai, China, during the period from September 2010 to December 2012.

Additionally, we gathered tumor specimens from 29 patients with HCC who underwent treatment with anti-PD-1 antibodies at Zhongshan Hospital, Fudan University, Shanghai, China, from August 2018 to September 2020. Treatment response to anti-PD-1 therapy was assessed in accordance with the Response Evaluation Criteria in Solid Tumors guidelines.[18] Written informed consent was obtained from the patients, and samples were used with approval from the Institutional Review Board of Zhongshan Hospital, Fudan University.

Single-cell RNA sequencing analyses

Single-cell RNA sequencing data of patients with HCC was obtained from Sun *et al*[19] (18 patients, Data set 1) and Zhang *et al*[20] (6 patients, Data set 2). Raw count matrices were then merged and analyzed using the Seurat R package (V.4.0.1).[21] Quality control steps included the removal of doublets and cells with >5% mitochondrial gene. Counts for the remaining cells were normalized against library size and regressed to correct for the unwanted cycling bias among proliferating cells, using S and G2M phase scores calculated by the CellCycleScoring function in the Seurat

package. Scaled and centered read counts were used as gene expression for further analysis. To visualize inferred cell clusters, t-distributed stochastic neighbor embedding (t-SNE) was applied based on the top 50 principal components. Automatic immune cell annotation was performed using the SingleR package. We carried out manual inspections to calibrate the automatic cell annotations by examining the most highly expressed marker genes between clusters and literature-derived and database-derived cell markers. The scores for pro-inflammatory and regulation of T-cell activation were calculated in the macrophage population at the single-cell level to assess phenotype shift. The genes for each score were defined in a previous study.[22] The differentially expressed genes between intratumoral and peritumoral macrophages, or PLA2G7^{low} and PLA2G7^{high} intratumoral macrophages were determined by using the FindMarkers function of the Seurat pipeline. All statistical analyses were conducted using R software (V.4.2.2).

Immunohistochemistry and immunofluorescence

Immunohistochemistry (IHC) and immunofluorescence (IF) analyses were conducted on paraffin-embedded human HCC tissue sections. Slides underwent deparaffinization in xylene followed by rehydration through a graded alcohol series. Antigen retrieval was accomplished by treating the slides with a citrate buffer at pH 6.0. Non-specific binding was blocked by incubating the slides with 5% bovine serum albumin (BSA), followed by overnight staining with primary antibodies against the following antigens at 4°C: PLA2G7 (Proteintech, #15526–1-AP), CD68 (Abcam, #ab283654), and CD8 (Abcam, #ab237709). In the case of IHC, horseradish-peroxidase-conjugated secondary antibodies (Vector Laboratories) were applied, followed by incubation with diaminobenzidine substrate (Vector Laboratories) and counterstaining with hematoxylin. In the context of IF, sections were exposed to secondary antibodies conjugated with Alexa Fluor 488 and 594 (diluted at 1:500, Invitrogen) for 1 hour at room temperature. Subsequently, slides were mounted using a medium containing DAPI (4',6-diamidino-2-phenylindole) and imaged under a fluorescence microscope (Olympus). Quantification of the mean fluorescence intensity was carried out using ImageJ software. Statistical analysis was performed using GraphPad Prism software.

Cell lines

The human HCC cell line MHCCLM3 was established in the Liver Cancer Institute of Zhongshan Hospital.[23] The human HCC cell line PLC/PRF/5 and the murine HCC cell line Hepa1-6 were acquired from the American Type Culture Collection. The human monocytic leukemia cell line THP-1 was sourced from the Stem Cell Bank, Chinese Academy of Sciences (Shanghai, China). The HCC cells and THP-1 cells were cultured in Dulbecco's Modified Eagle's Medium (DMEM, Gibco/Invitrogen) and Roswell Park Memorial Institute (RPMI) 1640 medium, respectively. Both media were supplemented with 10% fetal bovine serum (FBS, Gibco) and 1% penicillin–streptomycin (Invitrogen).

Small interfering RNA transfection

To knockdown PLA2G7 expression, DNA oligos targeting PLA2G7 were synthesized with the following sequences: siPLA2G7-1 (CGUUGGUUGUACAGACUUAAUTT) and siPLA2G7-2 (GGACCAAUCUGCUGCAGAAAUTT). Macrophages were transfected with either the small interfering RNAs (siRNAs) or negative control using Lipo8000 Transfection Reagent following the manufacturer's instructions (Beyotime, #C0533). Subsequent experiments were conducted on macrophages 48 hours after transfection.

Cell proliferation and migration assays

The cell proliferation assay was conducted using a CCK-8 Kit (Yeasen, Shanghai, China). Briefly, cells were seeded into 96-well plates (3,000 cells/well) and treated with various concentrations of darapladib (0.5 µM, 1 µM and 2 µM). At each time point (24, 48, and 72 hours), 10 µL of CCK-8 solution was added to 100 µL of culture media in each well, followed by incubation at 37°C for 2 hours. Absorbance was measured using a Multiskan Spectrum spectrophotometer (Thermo Scientific) at a wavelength of 450 nm. Cell migration was assessed using the wound healing test, where 5×10^5 cells were seeded into a well of a 6-well plate. The cell monolayers were mechanically disrupted using a sterile 20 µL micropipette tip to create a linear wound. The average distance migrated by the cells was measured using a microscope calibrated with an ocular micrometer.

Generation of primary macrophages with TAM-like characteristics

Euthanasia was performed on C57BL/6 mice, followed by aseptic flushing of their femurs and tibias using DMEM medium (Gibco) to procure bone marrow cells via syringe aspiration. Subsequent to lysing red blood cells, bone marrow (BM) cells were cultured in DMEM medium (Gibco) supplemented with 10% FBS (Gibco) and 20 ng/mL mouse macrophage colony-stimulating factor (M-CSF) (Absin, #abs04383) for a duration of 5 days to generate bone marrow-derived macrophages (BMDMs). The generated BMDMs were subsequently exposed to a conditioned medium originating from a murine HCC cell line (Hepa 1–6 cells) for a period of 24 hours, facilitating the induction of polarization towards a TAM phenotype.

RNA isolation and quantitative real-time PCR

Total RNA isolation was performed by processing the cells through the RNAeasy Animal RNA Isolation Kit with Spin Column (Beyotime, #R0027). The acquired RNA was then converted into complementary DNA (cDNA) using the 4 EZscript Reverse Transcription Mix II (EZBioscience, #EZB-RT2). Subsequent to that, quantitative PCR (qPCR) analysis was performed on the resultant single-stranded

cDNA using the 2 SYBR Green qPCR Master Mix (ROX2 plus) (EZBioscience, A0001). To ensure precision, each reaction was replicated in triplicate. β-actin was employed as the internal control. Primer sequences used in this study are available in online supplemental table S1.

Western blot assay

Protein extraction involved treating the samples witpheh radio-immunoprecipitation assay lysis buffer and Beyotime phenylmethanesulfonyl fluoride. Subsequently, the mixture was centrifuged at 14,000 rpm for 20 min at 4°C. Protein quantification was performed through a Beyotime BCA protein assay. The protein samples were then mixed with a 1×loading buffer and boiled for 8–10 min. Protein separation used 10% Sodium Dodecyl Sulfate Polyacrylamide Gel Electrophoresis, followed by electroblotting onto 0.2 µm polyvinylidene difluoride membranes from Millipore. Membranes were blocked using Protein Free Rapid Blocking Buffer (EpiZyme Biotechnology) for 15 min to prevent non-specific binding. For antibody detection, the membranes were incubated overnight at 4°C with primary antibodies, followed by a 1-hour incubation with secondary antibodies at room temperature. Protein band visualization used Ncm-ECL Ultra from New Cell and Molecular Biotech. The primary antibodies are summarized in online supplemental table S2.

Co-culture assay

Isolation of CD8 T cells from the spleens of wild-type C57BL/6 mice was carried out using the CD8 T Cell Isolation Kit (BioLegend, #480035) in accordance with the manufacturer's instructions. For preactivation, purified CD8 T cells were quantified and seeded onto a flat-bottom 96-well culture plate precoated with 2 µg/mL of anti-CD3 antibody (BioLegend, #100340) and 2 µg/mL of anti-CD28 antibody (BioLegend, #102116). The cells were cultured in a comprehensive medium comprising RPMI 1640, supplemented with 10% FBS, 100 U/mL interleukin-2 (Peprotech, #212–12), 2 mM L-glutamine (STEMCELL Technologies, #07100), 50 µM β-mercaptoethanol (GENOM Biotech, #GNM21985-1), 1 mM sodium pyruvate (Beyotime, C0331), 100 µM MEM non-essential amino acid (STEMCELL Technologies, #07600), and 10 mM HEPES (STEMCELL Technologies, #07200). After 24 hours, the CD8 T cells were co-cultured with macrophages at a 1:1 ratio. Following an additional 48-hour co-culture period, CD8 T cells were subjected to staining for interferon-γ (IFN-γ) and granzyme B (GZMB) to assess their activation status.

Flow cytometry

Cells were initially treated with an Fc receptor blocker for 10 min at room temperature to minimize non-specific binding. Following this, cells were subjected to a 30 min incubation at 4°C with monoclonal antibodies labeled with fluorescence, specifically designed to target desired surface markers. After completing the surface staining, the cells were fixed with 4% paraformaldehyde and permeabilized using 0.1% Triton X-100 in phosphate buffer solution (PBS) to facilitate intracellular staining. Subsequently, the cells were incubated in the dark at 4°C for 30 min with fluorochrome-conjugated antibodies that were specific to the desired intracellular markers. The antibodies employed are listed as follows: anti-CD86 (BioLegend, Clone#BU63 for human, Clone#GL-1 for mouse), anti-CD206 (BioLegend, Clone#15–2 for human, Clone#C068C2 for mouse), anti-MHC-II (BioLegend, Clone#M5/114.15.2), anti-granzyme B (eBioscience, Clone#NGZB), and anti-IFN-γ (BioLegend, Clone#XMG1.2). Finally, labeled cells underwent two washes with fluorescence-activated cell sorting buffer and were subsequently analyzed using a BD FACSCantoII Analyzer (BD Biosciences) in conjunction with FlowJo software (V.10.4).

Animal studies

Male C57BL/6 mice aged 6–7 weeks were employed in this study. In the subcutaneous HCC model, 100 µL of a single-cell suspension comprising 5×10^6 Hepa 1–6 cells in 1×PBS was injected into the right flank of each mouse. Tumor dimensions were assessed every 2 days using the formula: length×width^2×0.5 (mm^3). In the orthotopic HCC model, mice were anesthetized before orthotopic tumor cell implantation. An 8 mm transverse incision was created in the upper abdomen, followed by injecting a 25 µL single-cell suspension of Hepa 1–6 cells (2×10^6 per mouse), prepared with a 1:1 ratio of Matrigel (Corning, #356234) and 1×PBS, into the left hepatic lobe of the recipient C57BL/6 mouse using a microsyringe. Tumor weight was assessed at the conclusion of the study.

Once palpable, the following treatment commenced and mice were randomly divided into four groups (n=5 per group): For in vivo inhibition of PLA2G7, mice were intraperitoneally injected with darapladib at a dose of 10 mg/kg (MedChemExpress, #HY-111621) or vehicle control daily. For macrophage depletion, mice were injected with clodronate-containing liposomes (100 µL/injection, Yeasen, #40337ES10) beginning 2 days prior to tumor cell implantation and continuing every 4th day until the endpoint. In the case of anti-PD-1 therapy, mice were intraperitoneally treated with anti-mouse PD-1 antibody (200 µg per injection, Bio X Cell, #BP0146) or IgG isotype control every 3rd day. All animal experiments were conducted in accordance with the guidelines of the Shanghai Medical Experimental Animal Care Commission and received approval from the Ethical Committee on Animal Experiments of the Animal Care Committee of Zhongshan Hospital, Fudan University.

Multiplex immunofluorescence assay

Tissue slides were initially deparaffinized using xylene and subsequently rehydrated through a series of graded ethanol solutions. To quench endogenous peroxidases, 0.3% hydrogen peroxide was employed, and antigen retrieval was achieved using a citrate buffer. Following these steps, the slides were shielded with a 5% BSA solution to

reduce non-specific binding. Primary antibodies specific to PLA2G7 (Proteintech, #15526–1-AP), CD68 (Abcam, #ab955), CD3 (Abcam, #ab16669), CD20 (Abcam, #ab9475 for human; Abclonal, #A1793 for mouse), F4/80 (Cell Signaling Technology, #70076T), MHC-II (Abcam, #ab23990), and CD8 (Abcam, #ab217344) were applied to the slides and incubated at 37°C in a humidified chamber for 60 min. After a buffer wash, corresponding horseradish peroxidase-conjugated secondary antibodies were applied and incubated at room temperature for 45 min. Subsequently, the slides underwent another wash to remove unbound antibodies before proceeding to the next stage. Finally, the slides were stained with a DAPI solution at 37°C for 10 min in the absence of light to facilitate nucleus visualization.

Statistical analysis

Group differences were assessed using either the Student's t-test or the Mann-Whitney U test, depending on the data distribution. Differences in constituent ratios between groups were assessed using either the χ^2 test or Fisher's exact test, depending on sample size and expected cell frequencies. Survival curves were generated using the Kaplan-Meier method, and group differences were assessed using the log-rank test. Independent prognostic factors were identified using a Cox proportional hazards regression model. Statistical analyses were performed using R software (V.4.2.2) or GraphPad Prism (V.9.1.1, San Diego, California, USA). Results were reported as not significant or with asterisks denoting the level of significance: *p<0.05, **p<0.01, ***p<0.001.

RESULTS

Single-cell RNA sequencing analyses identify valuable intratumoral macrophage-specific marker genes associated with prognosis in HCC

Two publicly available data sets comprising single-cell RNA sequencing data from patients with HCC, obtained from Sun *et al*[19] (18 patients, Data set 1) and Zhang *et al*[20] (6 patients, Data set 2), were used for bioinformatics analyses within this study. In Data set 1, we identified 24 cell subclusters and annotated them into 10 cell types using canonical marker genes, encompassing T cells, tumor cells, monocytes, dendritic cells (DCs), endothelial cells, epithelial cells, macrophages, B cells, hematopoietic stem cells, and natural killer (NK) cells (figure 1A). In Data set 2, we delineated 14 cell subclusters and classified them into 8 distinct cell types based on canonical marker genes, including T cells, DCs, innate lymphoid cells, B cells, macrophages, mast cells, monocytes, and NK cells (figure 1B). Despite the diversity of cell types in HCC, macrophages play a crucial role in modulating immune responses within the TME. As such, we extracted 286 and 822 macrophage-specific marker genes from Data set 1 and Data set 2, respectively, for further examination. Subsequently, to elucidate differences in macrophages between tumor and adjacent normal tissues, we conducted a comparative analysis between intratumoral and peritumoral macrophages. This analysis unveiled a spectrum of differentially expressed genes (DEGs) identified through the use of the FindMarkers function (949 genes in Data set 1; 709 genes in Data set 2). Gene set enrichment analysis (GSEA) revealed that these DEGs were primarily associated with innate and adaptive immune responses, phagocytosis, and inflammatory processes in both cohorts (figure 1C,D). By intersecting the macrophage-specific gene sets with the DEGs identified between tumor-infiltrating and adjacent normal tissue-derived macrophages in both cohorts, we identified 34 potentially influential genes that could contribute to the macrophage-mediated immunosuppressive TME in HCC (figure 1E). To further evaluate the clinical significance of these genes, we conducted the least absolute shrinkage and selection operator analysis within the TCGA-LIHC cohort, which included 374 patients with HCC (figure 1F,G). These analyses ultimately identified seven highly significant genes (CTSL, NPL, CPVL, APOE, TTYH3, S100A9, and PLA2G7), supported by 1000-fold cross-validation (figure 1H). In summary, our analyses reveal a panel of genes that may contribute to macrophage-mediated immunosuppression and impact the prognosis of HCC.

PLA2G7 is upregulated in HCC tissues and mainly expressed in intratumoral macrophages

Subsequently, we employed Bubble and t-SNE plots to visualize the distribution of gene expression among distinct single-cell subclusters. Our findings specifically revealed that PLA2G7 exhibited high expression in macrophages, moderate expression in monocytes and DCs, and minimal expression in other cell types (figure 2A–D). This observation was corroborated by additional single-cell data sets from patients with HCC (GSE146115, GSE146409, and GSE125449) (online supplemental figure S1). Moreover, a multiplex immunofluorescence (mIF) assay demonstrated the predominant co-localization of PLA2G7 with $CD68^+$ macrophages, as opposed to other critical immune cell types including $CD3^+$ T cells and $CD20^+$ B cells, in human HCC tissues (online supplemental figure S2). As a result, we prioritized this molecule for further analysis. Our data suggested a significant increase in PLA2G7 expression in tumor-infiltrating macrophages compared with macrophages from adjacent normal tissues, blood, and ascites (figure 2E,F). Additionally, through the analysis of two bulk transcriptome data sets from patients with HCC (TCGA-LIHC and GSE14520), we verified the upregulation of PLA2G7 levels in tumor tissues compared with peritumor tissues (online supplemental figure S3). Subsequently, we performed IHC staining on an HCC cohort from our institution (Zhongshan Cohort). Although no significant differences were detected in CD68 expression levels between the tumor and adjacent normal tissues, we did observe increased PLA2G7 expression in tumor tissues (figure 2G,H). In summary, these findings collectively suggest the upregulation of PLA2G7

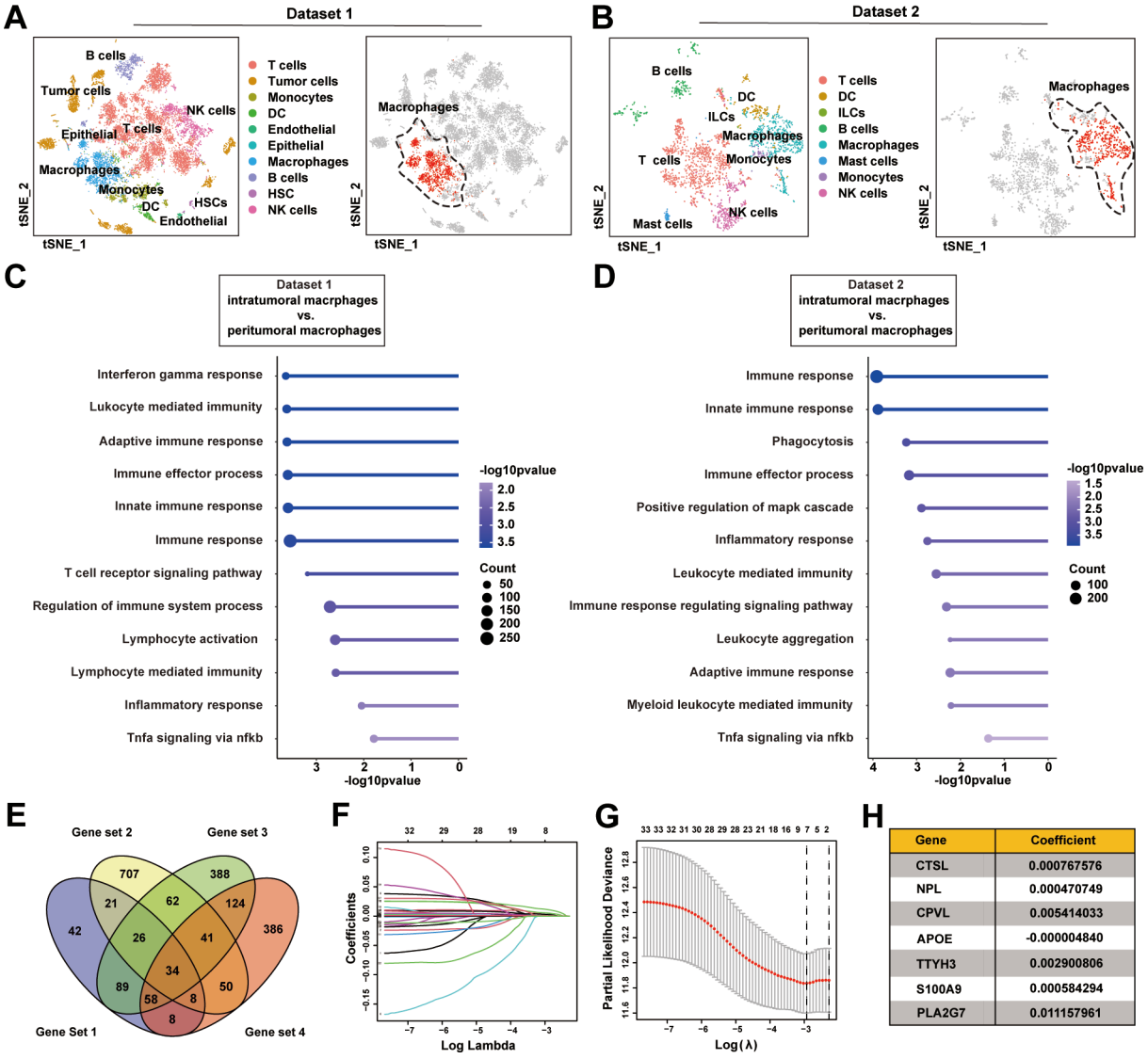

Figure 1 Single-cell RNA sequencing analyses identify valuable intratumoral macrophage-specific marker genes associated with prognosis in HCC. (A) t-SNE plots for distinct cell subsets in Data set 1 (left panel). The macrophage population was highlighted in red color (right panel). (B) t-SNE plots for distinct cell subsets in Data set 2 (left panel). The macrophage population was highlighted in red color (right panel). (C) GSEA enrichment analysis of intatumoral versus peritumoral macrophages using scRNA-seq from Data set 1. (D) GSEA enrichment analysis of intatumoral versus peritumoral macrophages using scRNA-seq data from Data set 2. (E) Venn diagram showing the intersection of macrophage-specific gene sets (Gene set 1 from Data set 1; Gene set 3 from Data set 2) with the DEGs (Gene set 3 from Data set 1; Gene set 4 from Data set 2) identified between intratumoral and peritumoral macrophages. (F–H) Identification of the most valuable intratumoral macrophage-specific genes associated with prognosis in HCC using the LASSO analysis with 1000-fold cross-validation in TCGA-LIHC cohort. DC, dendritic cell; DEGs, differentially expressed genes; GSEA, gene set enrichment analysis; HCC, hepatocellular carcinoma; HSC, hematopoietic stem cell; ILCs, innate lymphoid cells; LASSO, least absolute shrinkage and selection operator; NK, natural killer; scRNA-seq, single-cell RNA sequencing; TCGA-LIHC, The Cancer Genome Atlas liver hepatocellular carcinoma; t-SNE, t-distributed stochastic neighbor embedding.

in HCC and its predominant expression within intratumoral macrophages.

Macrophage-specific PLA2G7 is significantly correlated with prognosis and immunotherapy response in patients with HCC

Subsequently, we evaluated the prognostic significance of PLA2G7 in patients with HCC. In the Zhongshan Cohort, our analysis unveiled a significantly shorter overall survival (OS) in the PLA2G7-high group compared with the PLA2G7-low group (figure 3A,B). Additionally, we conducted subgroup analysis on patients with HCC with diverse oncogenic etiologies. No significant differences in survival were observed between patients with HCC with hepatitis virus infection and those with spontaneous HCC (online supplemental figure S4A). Notably, spontaneous HCC exhibited higher levels of tumorous PLA2G7 expression compared with hepatitis virus-induced HCC (online supplemental figure S4B). Although the levels

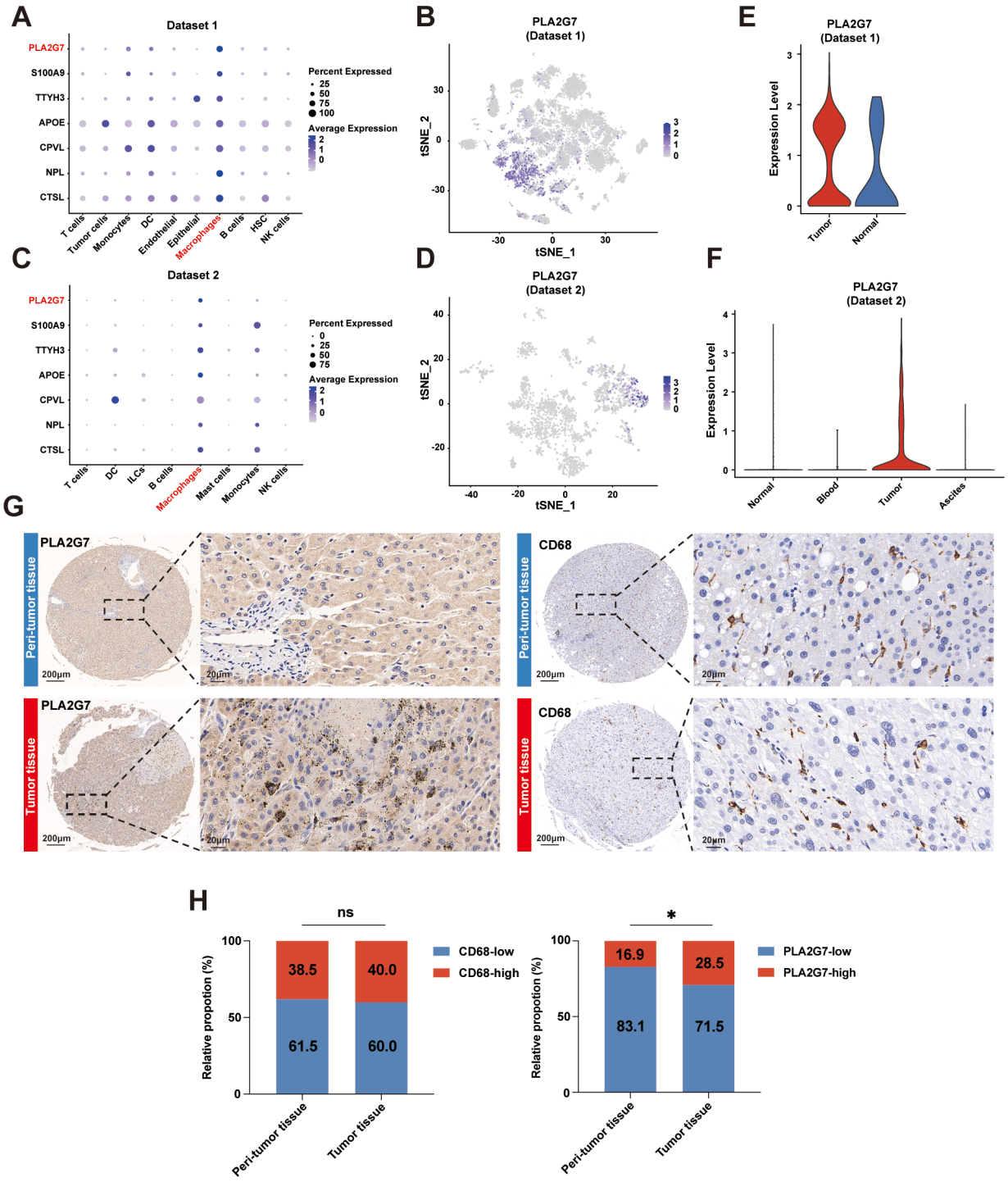

Figure 2 PLA2G7 is upregulated in HCC tissues and mainly expressed in intratumoral macrophages. (A) Bubble plot of the expression levels of the seven genes in each single cell subcluster in Data set 1. (B) t-SNE plot of all single cells colored by the expression level of PLA2G7 in Data set 1. (C) Bubble plot of the expression levels of the seven genes in each single cell subcluster in Data set 2. (D) t-SNE plot of all single cells colored by the expression level of PLA2G7 in Data set 2. (E) The violin plot displaying the expression levels of PLA2G7 in macrophage from tumor and adjacent normal tissues in Data set 1. (F) The violin plot displaying the expression levels of PLA2G7 in macrophage from tumor, adjacent normal tissues, blood, and ascites in Data set 2. (G) Representative IHC images of PLA2G7 and CD68 in HCC tissues and peritumor tissues. Scale bar: 200 μm (left) and 20 μm (right). (H) IHC expression pattern of CD68 (left panel) and PLA2G7 (right panel) in HCC tissues versus peritumor tissues (n=130). χ^2. ns, no significance; *p<0.05. HCC, hepatocellular carcinoma; IHC, immunohistochemistry; PLA2G7, phospholipase A2 Group VII; t-SNE, t-distributed stochastic neighbor embedding.

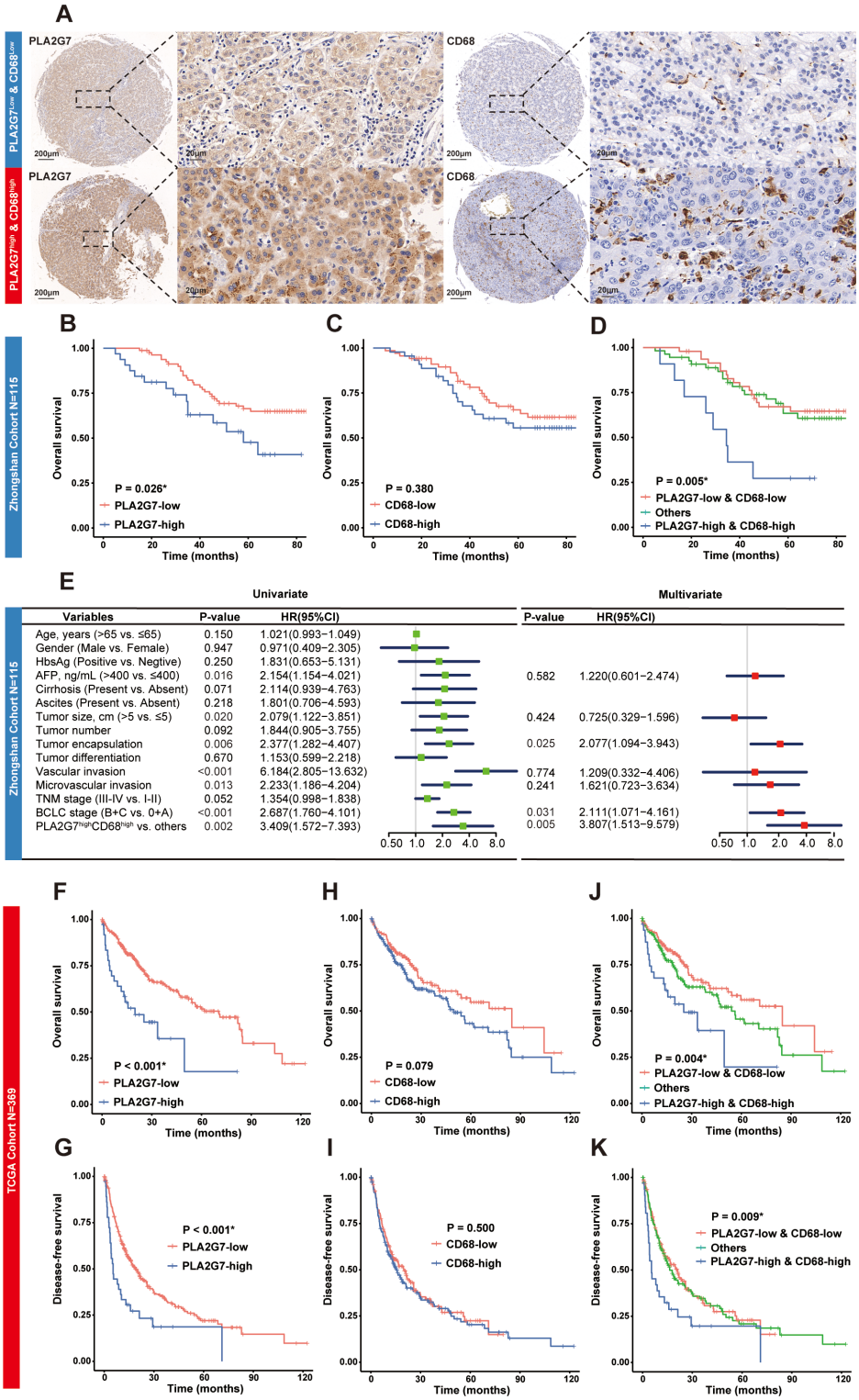

Figure 3 The prognostic value of macrophage-specific PLA2G7 in HCC. (A) Representative IHC images of low-expressions and high-expressions of PLA2G7 and CD68 in HCC tissues. Scale bar: 200 µm (left) and 20 µm (right). (B–C) OS curves for patients with HCC with low-expression and high-expression of PLA2G7 or CD68 in the Zhongshan cohort (n=115). (D) OS curves for patients with HCC with low-co-expressions and high-co-expressions of PLA2G7/CD68 in the Zhongshan cohort (n=115). (E) Forest plots for univariate and multivariate Cox proportional hazards regression models of OS in the Zhongshan cohort. (F–I) OS and DFS curves for patients with HCC with low-mRNA and high-mRNA levels of PLA2G7 or CD68 in TCGA-LIHC cohort (n=369). (J–K) OS and DFS curves for patients with HCC with low-co-expressions and high-co-expressions of PLA2G7/CD68 in TCGA-LIHC cohort (n=369). Log-rank test. * indicates statistical significance. AFP, α-fetoprotein; BCLC, Barcelona Clinic Liver Cancer; DFS, disease-free survival; HBsAg, hepatitis B surface antigen; HCC, hepatocellular carcinoma; IHC, immunohistochemistry; mRNA, messenger RNA; OS, overall survival; PLA2G7, phospholipase A2 Group VII; TCGA-LIHC, The Cancer Genome Atlas liver hepatocellular carcinoma; TNM, tumor-nodes-metastasis.

of PLA2G7 expression could differentiate the survival curves in both subgroups of patients with HCC, statistical significance was not achieved in the spontaneous HCC group (online supplemental figure S4C).

Contrastingly, no significant differences in survival were found between the CD68-low and CD68-high groups (figure 3C). Notably, our analysis indicated that patients with HCC with elevated expressions of both PLA2G7 and CD68 exhibited the lowest OS rates (figure 3D). Moreover, the Cox proportional hazard regression models demonstrated that high intratumoral expression of both PLA2G7 and CD68 independently predicted the risk for OS within our HCC cohort (figure 3E). Our findings were consistently supported by the TCGA-LIHC cohort, where elevated PLA2G7 expression correlated with reduced OS and disease-free survival (DFS) (figure 3F,G), whereas CD68 expression did not exhibit a similar correlation (figure 3H,I). Remarkably, patients with HCC with elevated levels of both PLA2G7 and CD68 experienced the most adverse outcomes in both OS and DFS (figure 3J,K). In summary, macrophage-specific PLA2G7 emerges as a significant adverse prognostic factor in patients with HCC.

Numerous studies consistently demonstrate that intratumoral macrophages act as substantial barriers to ICB therapy by inhibiting the activation of effector T cells or impeding their infiltration into the TME.[8] Therefore, we explored the potential role of PLA2G7 in immunotherapy resistance among patients with HCC. We collected a cohort of 29 patients with HCC undergoing anti-PD-1 antibody treatment for IF staining (figure 4A–D). Our results showed a significant decrease in PLA2G7 and CD68 expression in patients with a partial response compared with those with progressive disease (online supplemental figure S5). Additionally, we revealed that patients with elevated levels of both PLA2G7 and CD68 had significantly reduced CD8 T-cell infiltration (figure 4E), impaired responses to anti-PD-1 treatment (figure 4F), and worse OS (figure 4G) compared with other patients. These findings suggest that PLA2G7 is not only associated with the prognosis of patients with HCC but also has implications for T-cell immunity and ICB responses.

PLA2G7 plays a pivotal role in preserving the immunosuppressive phenotype in macrophages

Next, we used single-cell RNA sequencing data from patients with HCC (Data set 1) to investigate the role of PLA2G7^{high} macrophages in the HCC microenvironment. We divided 1773 intratumoral macrophages into PLA2G7-low (n=887) and PLA2G7-high (n=886) groups based on the median PLA2G7 expression (figure 5A). GSEA showed that PLA2G7^{high} macrophages were significantly associated with reduced activity in antigen processing and presentation, lymphocyte chemotaxis, and regulation of T-cell activation, in comparison to PLA2G7^{low} macrophages (online supplemental figure S6A). Next, we assessed macrophage function using established gene signatures related to pro-inflammatory response and T-cell activation regulation.[22] PLA2G7^{high} macrophages showed significantly lower scores in both pro-inflammatory and T-cell activation compared with their PLA2G7^{low} counterparts (figure 5B). In particular, pro-inflammatory marker genes, such as IL1B, TNF, NOS2, CX3CR1, and CSF1R (online supplemental figure S6B), and genes associated with T-cell activation, such as CXCL2, CCL8, CCL5, and CCL2 (online supplemental figure S6C), were downregulated in PLA2G7^{high} macrophages.

We then investigate whether PLA2G7 plays a functional role in macrophages. Initially, THP-1-differentiated macrophages were used in vitro. Treatment with tumor-conditioned medium (TCM) from human HCC cells significantly upregulated PLA2G7 expression in macrophages (figure 5C). Intriguingly, silencing PLA2G7 in TCM-educated macrophages using siRNA polarized macrophages towards an M1 phenotype, as indicated by the increased ratio of CD86, an M1 marker, to CD206, an M2 marker (online supplemental figure S7). Next, we applied darapladib, the most advanced and highly selective inhibitor of Lp-PLA2 (encoded by the PLA2G7 gene), and observed a consistent shift in macrophage phenotype (figure 5D). Of note, this treatment is insufficient to induce alterations in the proliferation and migration capabilities of human HCC cells (online supplemental figure S8).

Subsequently, primary mouse BMDMs were employed to validate the potential of inhibiting PLA2G7 in mitigating the immunosuppressive features of macrophages. BMDMs were isolated and exposed to a TCM derived from cultured Hepa 1–6 cells[24] (figure 5E). These TAM-like BMDMs exhibited a significantly increased PLA2G7 levels (figure 5F), accompanied by an M2 immunosuppressive phenotype, characterized by increased expression of Arg, Fizz, and Il10, along with reduced expression of Il1b, Il6, Il12, and Tnfa (online supplemental figure S9A). After treating TAMs with darapladib, we observed an increase in the expression of immunostimulatory genes and a simultaneous decrease in immunosuppressive genes (online supplemental figure S9B). Flow cytometric analysis further showed that darapladib induced a shift of TAMs towards an M1 phenotype, as evidenced by the increased CD86 to CD206 ratio (figure 5G). Next, we conducted in vitro co-culture experiments with TAMs and splenic CD8 T cells. Our data demonstrated that darapladib treatment significantly increased the ability of TAMs to activate CD8 T cells, as indicated by elevated levels of cytotoxic effector molecules, including IFN-γ and GZMB (figure 5H). In summary, these data suggest that PLA2G7^{high} macrophages represent a subtype characterized by a highly immunosuppressive phenotype in the HCC microenvironment. Inhibition of PLA2G7 by darapladib prompts macrophages to adopt an immunostimulatory phenotype capable of supporting CD8 T-cell activation.

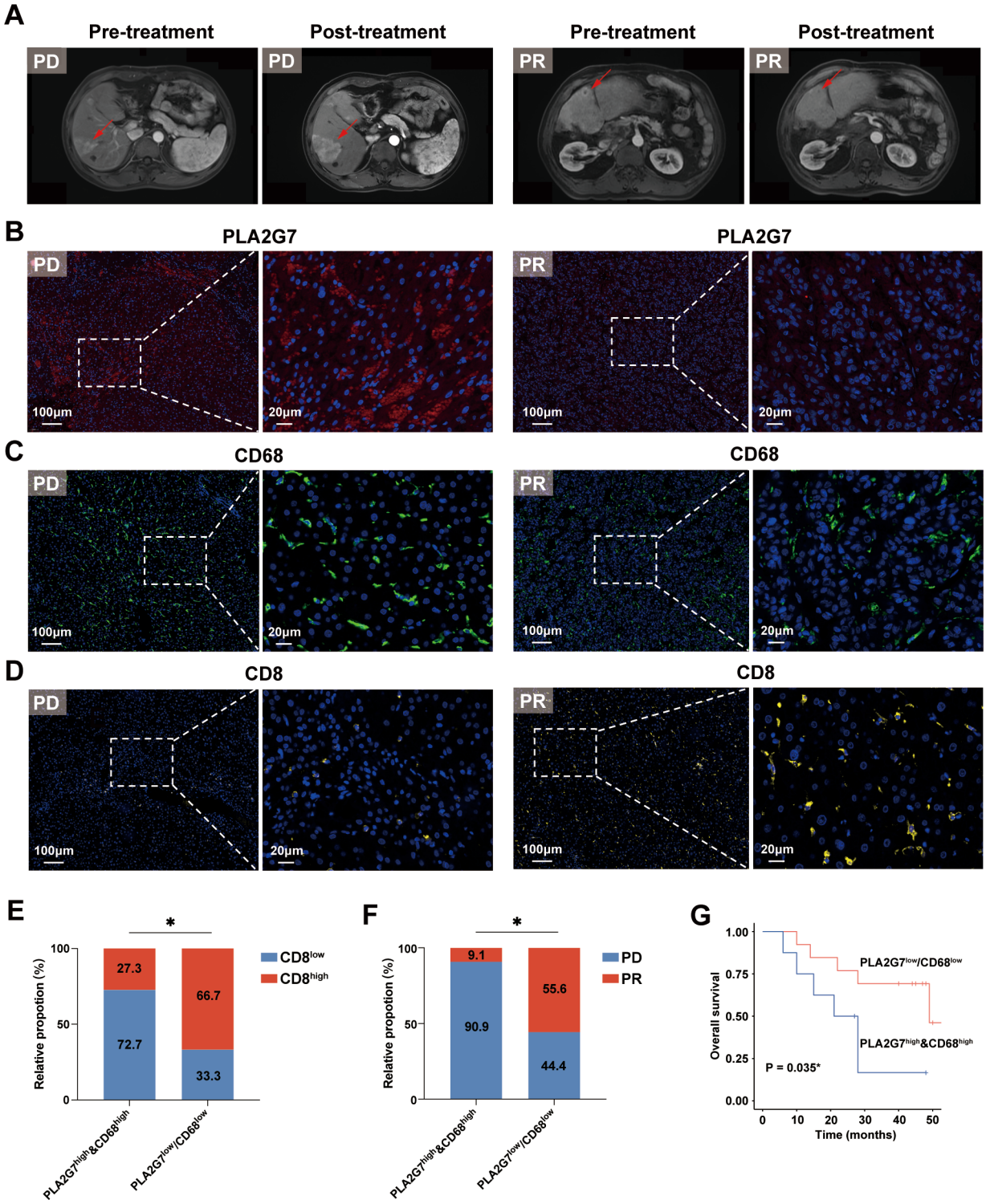

Figure 4 The association between macrophage-specific PLA2G7 and immunotherapy response in patients with HCC receiving anti-PD-1 treatment. (A) Representative MRIs of patients with HCC receiving anti-PD-1 treatment with PD and PR. (B–D) Representative IF images depicting the expressions of PLA2G7, CD68, and CD8 in tumor tissues from patients with HCC with PD and PR. Scale bar: 100 µm (left) and 20 µm (right). (E) Expression pattern of CD8 among patients with anti-PD-1 treated HCC with PLA2G7^{high}&CD68^{high} versus others (n=29). (F) The distributions of treatment responses among patients with anti-PD-1 treated HCC with PLA2G7^{high}&CD68^{high} versus others (n=29). (G) Kaplan-Meier analysis comparing the overall survival of patients with anti-PD-1 treated HCC with PLA2G7^{high}&CD68^{high} versus others (n=21). Statistical analysis was performed using the χ^2 test in (E) the Fisher's exact test in (F) and the log-rank test in (G). *p<0.05. HCC, hepatocellular carcinoma; IF, immunofluorescence; PD, progressive disease; PD-1, programmed cell death protein 1; PLA2G7, phospholipase A2 Group VII; PR, partial response.

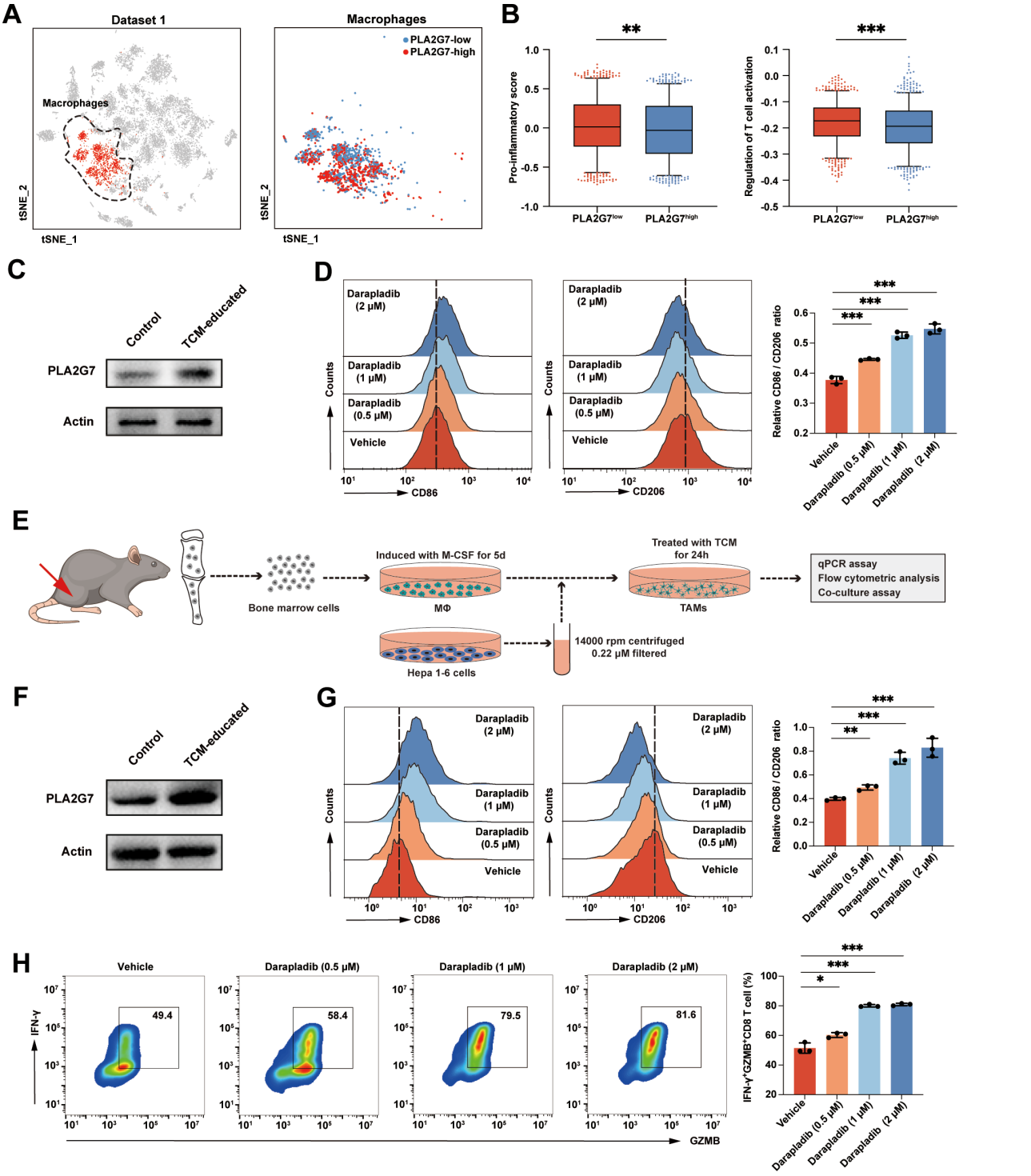

Figure 5 PLA2G7 preserves the immunosuppressive phenotype in macrophages. (A) t-SNE plots showing the PLA2G7^{low} and PLA2G7^{high} macrophages in Data set 1. (B) The expression-based scores for pro-inflammation (left panel) and T-cell activation (right panel) were calculated in PLA2G7^{low} and PLA2G7^{high} macrophages at the single-cell level. (C) Western blot analysis of PLA2G7 in untreated or TCM-educated THP-1-differentiated macrophages. β-actin was used as loading control. (D) Flow cytometric analysis of CD86 and CD206 on TCM-education THP-1-differentiated macrophages treated with darapladib (0.5 μM, 1 μM, and 2 μM) or vehicle. (E) Schematic representation of in vitro induction of TAM-like BMDMs. (F) Western blot analysis of PLA2G7 in untreated or TCM-educated BMDMs. β-actin was used as loading control. (G) Flow cytometric analysis of CD86 and CD206 on TCM-educated BMDMs treated with either darapladib (0.5 μM, 1 μM, and 2 μM) or vehicle. (H) Analysis of IFN-γ+ GZMB+ CD8 T cells after co-culturing with TCM-educated BMDMs treated with either darapladib (0.5 μM, 1 μM, and 2 μM) or vehicle. Statistical analysis was performed using the Mann-Whitney U test in (B) and the Student's t-test in (D) and (G–H). Data was presented as median with IQR in (B) and mean with SD in (D) and (G–H). *p<0.05, **p<0.01, ***p<0.001. BMDM, bone marrow-derived macrophages; GZMB, granzyme; IFN-γ, interferon-γ; PLA2G7, phospholipase A2 Group VII; TCM, tumor-conditioned medium; t-SNE, t-distributed stochastic neighbor embedding.

PLA2G7 promotes macrophage phenotypic transition via modulating the NF-κB pathway

Subsequently, we explored the molecular mechanisms through which PLA2G7 regulated the phenotypic transition of macrophages. Our previous analysis of macrophages from patients with HCC revealed significant downregulation of classical inflammatory pathways, such as NF-κB and MAPK, in intratumoral macrophages compared with peritumoral macrophages (figure 1C,D). Interestingly, intratumoral macrophages with elevated PLA2G7 levels exhibited a significant decrease in the activity of NF-κB and MAPK pathways compared with their counterparts with lower PLA2G7 levels (figure 6A,B). Therefore, we hypothesized that PLA2G7 may sustain the immunosuppressive phenotype in macrophages by inactivating the NF-κB and MAPK pathways. Consistently, western blot experiments confirmed the activation of both the NF-κB and MAPK pathways when PLA2G7 was inhibited by darapladib in TAMs (figure 6C,D). Subsequently, we pretreated the macrophages with the NF-κB inhibitor JSH-23 or the MAPK inhibitor SB203580 before administering darapladib treatment, followed by flow cytometric analysis. Our findings indicated that the JSH-23 reversed the M1 polarization in TAMs induced by PLA2G7 inhibition, whereas the SB203580 did not show the same effect (figure 6E–G, online supplemental figure S10,S11). Moreover, the co-culture assay also validated that inhibiting the NF-κB pathway could reverse the immunostimulatory phenotype induced by darapladib (figure 6H,I). In summary, our results highlight that the PLA2G7 primarily induces TAM phenotypic transition by regulating the NF-κB pathway.

PLA2G7 inhibition by darapladib enhances the efficacy of anti-PD-1 treatment in HCC in vivo

To investigate the potential of inhibiting PLA2G7 to restrain tumor growth and enhance immunotherapy efficacy in HCC in vivo, we established murine orthotopic HCC models. Initially, by using mIF assay, we substantiated the predominant co-localization of PLA2G7 with F4/80^{+} macrophages in murine HCC (online supplemental figure S12). Furthermore, our data revealed a markedly elevated infiltration of PLA2G7^{high} macrophages within tumor tissues in comparison to peritumor tissues (online supplemental figure S13). Notably, these findings align consistently with our observations in human HCC samples.

By administering darapladib to HCC-bearing C57BL/6 mice, we observed a significant impediment to HCC growth. Notably, the depletion of macrophages abrogated the antitumor effects of darapladib, underscoring a dependence on macrophages for its efficacy (figure 7A, online supplemental figure S14). Subsequently, HCC-bearing mice were subjected to treatment with IgG, darapladib, anti-PD-1 antibody, or a combination of anti-PD-1 antibody and darapladib (figure 7A). Our results showed that darapladib, the anti-PD-1 antibody, and the combination therapy significantly inhibited the growth of HCC tumors. Simultaneously applying darapladib and anti-PD-1 resulted in the most substantial inhibition of HCC growth (figure 7B,C). The mIF analysis of murine orthotopic HCC samples demonstrated that darapladib alone significantly increased the infiltration of major histocompatibility complex (MHC)-II^{+} M1 macrophages and CD8^{+} T cells within tumors. Futhermore, the combination therapy exhibited significantly higher infiltrations of MHC-II^{+} M1 macrophages and CD8^{+} T cells compared with the monotherapy groups, while total macrophage infiltration showed no significant difference (figure 7E–G). The potential of darapladib to enhance immunotherapy efficacy was also validated using subcutaneous HCC models (figure 7H–J). In summary, these findings underscore the potential of darapladib, a PLA2G7 selective inhibitor, to enhance the therapeutic effectiveness of anti-PD-1 treatment in HCC.

DISCUSSION

Although anti-PD-1 therapy has demonstrated success in various solid tumors, its efficacy has been limited to a specific subgroup of patients with HCC. Macrophages represent a diverse population involved in complex and finely regulated interactions with other cellular elements within the HCC microenvironment, profoundly influencing the overall tumor immune landscape and modulating the response to immunotherapy.[8] Therefore, targeting macrophages has become one of the most favored strategies to complement ICB therapy in HCC. In this study, using multiple high-throughput single-cell analyses, we identified a previously undescribed PLA2G7^{high} macrophage subset and elucidated its immune association and clinical significance in HCC. Moreover, the inhibition of PLA2G7 effectively counteracts the immunosuppressive function of intratumoral macrophages, thereby improving the response to immunotherapy in HCC.

In recent times, PLA2G7's high expression in various tumors has been well-documented and linked to unfavorable prognoses.[13–17] Additionally, Lehtinen *et al* identified a subset of metastatic and aggressive breast cancers that exhibit heightened PLA2G7 expression, fostering epithelial-mesenchymal transition and migration in cultured breast cancer cells.[17] Zheng *et al*, in their work, demonstrated that suppressing PLA2G7 expression impedes the migration and proliferation of diffuse large B-cell lymphoma cells, while enhancing apoptotic cell death.[15] However, these studies have mainly concentrated on the direct impact of PLA2G7 on tumor cells, without thoroughly exploring its functions within the TME. In our study, using single-cell data analysis and mIF assays on human HCC tissues, we observed that PLA2G7 is primarily expressed in macrophages rather than in tumor cells or other immune cell types within the context of HCC. Furthermore, the expression of PLA2G7 in intratumoral macrophages is notably higher than in macrophages derived from adjacent normal tissues, serum, or ascites. Our findings suggest that PLA2G7^{high} macrophages

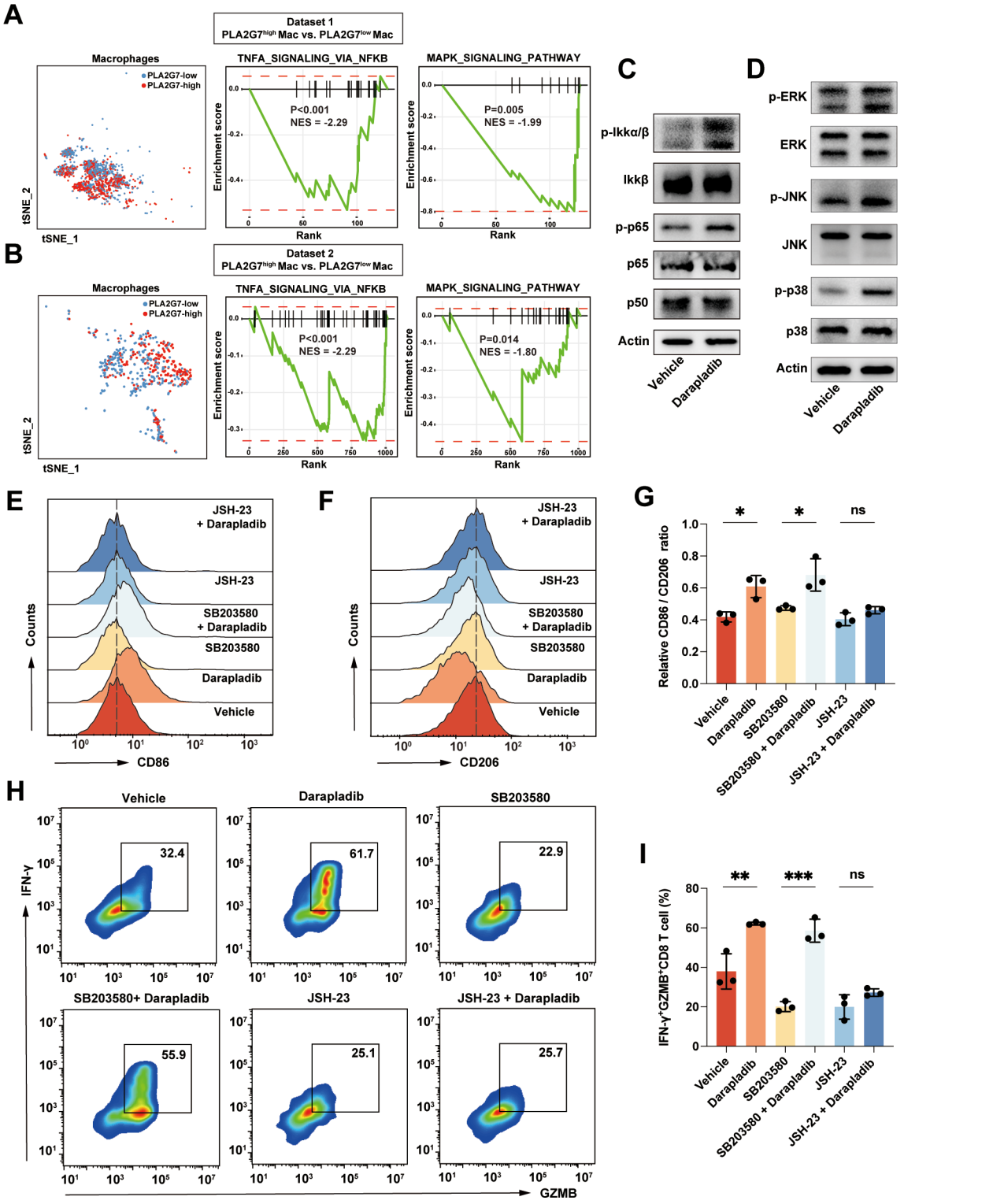

Figure 6 PLA2G7 promotes macrophage phenotypic transition via modulating the NF-κB pathway. (A–B) GSEA analysis demonstrates the downregulation of signature genes of NF-κB and MAPK pathways in PLA2G7^{high} macrophages versus PLA2G7^{low} macrophages in both Data set 1 (A) and Data set 2 (B). (C–D) Western blot analysis of NF-κB and MAPK pathways in tumor-associated macrophages treated with either darapladib (2 μM) or vehicle. (E–G) Flow cytometric analysis of CD86 and CD206 on TCM-educated BMDMs treated with either darapladib (2 μM), SB203580 (10 μM), SB203580 (10 μM) + darapladib (2 μM), JSH-23 (10 μM), JSH-23 (10 μM) + darapladib (2 μM), or vehicle. (H–I) Analysis of IFN-γ+ GZMB+ CD8 T cells after co-culturing with TCM-educated BMDMs treated with either darapladib (2 μM), SB203580 (10 μM), SB203580 (10 μM) + darapladib (2 μM), JSH-23 (10 μM), JSH-23 (10 μM) + darapladib (2 μM), or vehicle. Student's t-test. Data was presented as mean with SD. ns, no significance; *p<0.05, **p<0.01, ***p<0.001. BMDM, bone marrow-derived macrophages; GZMB, granzyme B; IFN-γ, interferon-γ; NES,normalized enrichment score; PLA2G7, phospholipase A2 Group VII; TCM, tumor-conditioned medium; t-SNE, t-distributed stochastic neighbor embedding.

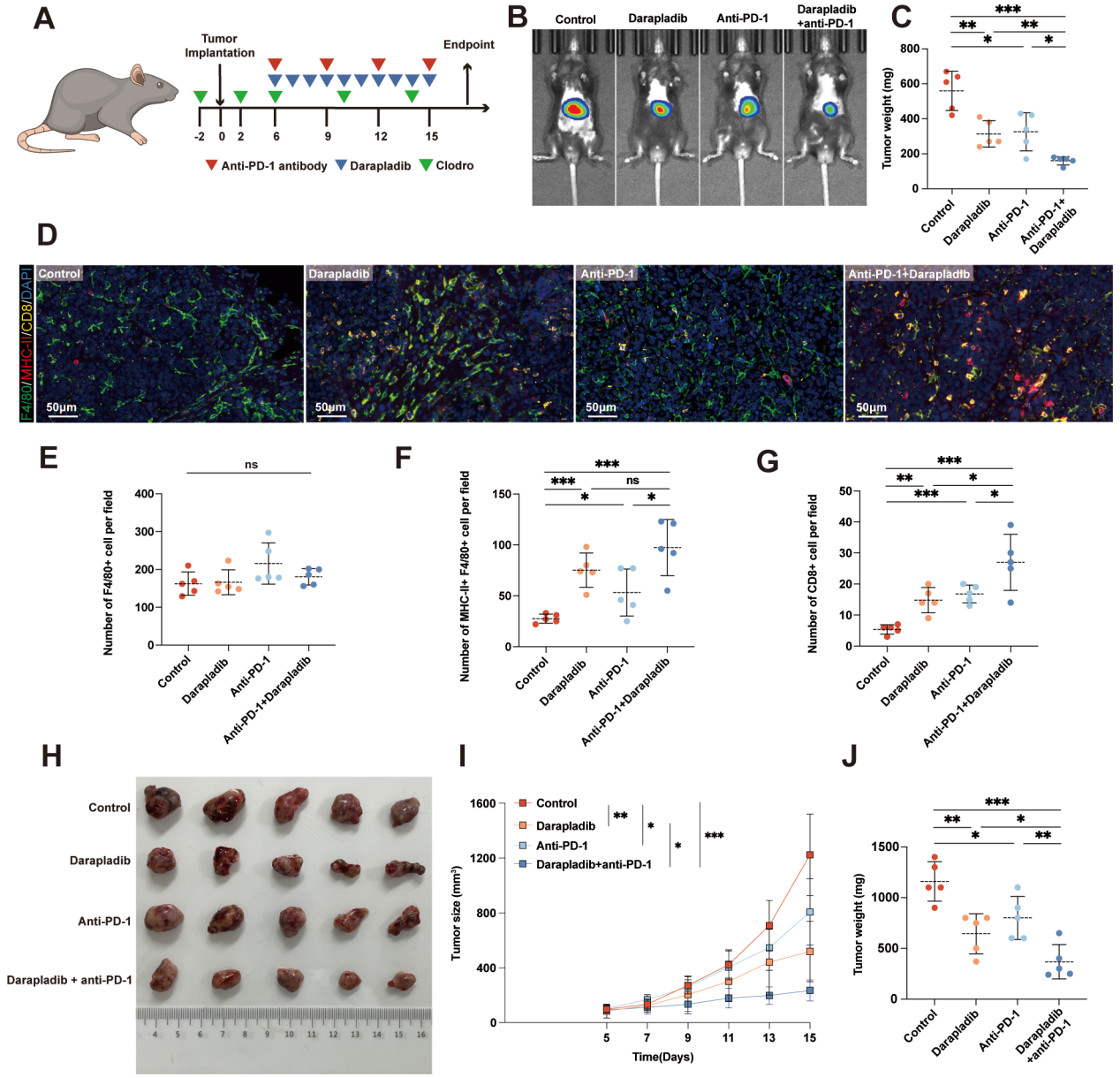

Figure 7 Phospholipase A2 Group VII inhibition by darapladib enhances the efficacy of anti-PD-1 treatment in HCC in vivo. (A) Schematic representation of the treatment schedule for clodronate liposomes, anti-PD-1 and darapladib in C57BL/6 mice bearing HCC tumors. (B–C) Murine orthotopic HCC tumors treated with either darapladib, anti-PD-1, darapladib+anti-PD-1, or isotype control. Representative bioluminescence images and statistical diagram illustrating tumor weights are presented (n=5, each). (D) Representative pictures of mIF analysis for F4/80, MHC-II, and CD8 markers in the orthotopic HCC tumors treated with either darapladib, anti-PD-1, darapladib+anti-PD-1, or isotype control. Scale bar: 50 μm. (E–G) Quantification of corresponding immune cells by mIF analysis. (H–J) Tumor growth curves and weights of Hepa 1–6 subcutaneous tumors in C57BL/6 mice treated with either darapladib, anti-PD-1, darapladib+anti-PD-1, or isotype control (n=5 each). Student's t-test (or one-way analysis of variance with a post hoc LSD test in (E)). Data was presented as mean with SD. ns, no significance; *p<0.05, **p<0.01, ***p<0.001. HCC, hepatocellular carcinoma; mIF, multiplex immunofluorescence; MHC, major histocompatibility complex; PD-1, programmed cell death protein 1; ROI, region of interest.

within HCC TME constitute a highly immunosuppressive subset characterized by reduced capacities of pro-inflammatory, antigen presentation, and T-cell activation. The clinical investigation further confirmed that patients with HCC with elevated levels of both PLA2G7 and CD68 expression experience poorer OS. In summary, our analysis unveiled a previously unidentified subset of macrophages characterized by elevated PLA2G7 expression and demonstrated its clinical relevance in the prognosis of patients with HCC.

Another significant finding in this study is the strong association between macrophage-specific PLA2G7 and a less favorable treatment response among patients with HCC undergoing anti-PD-1 therapy. This observation aligns with a prior investigation by Saenger *et al*, which identified PLA2G7 as a novel biomarker for predicting

immunotherapy responses in patients with melanoma.[16] The CD8 T cell is pivotal in immune checkpoint therapy,[25] and our study revealed that patients expressing both high levels of PLA2G7 and CD68 experienced reduced CD8 infiltration, likely contributing to their suboptimal response to ICB therapy. Through in vitro co-culture assay, we demonstrated that inhibiting PLA2G7 could reverse the immunosuppressive characteristics of TAMs and enhance their capacity to activate CD8 T cells. Moreover, using murine HCC models, we demonstrated that the administration of PLA2G7 inhibitor effectively inhibited tumor growth, accompanied by increased infiltrations of M1 macrophages and CD8 T cells. In summary, our findings identify PLA2G7 as a promising biomarker for predicting response to ICB therapy in patients with HCC. Moreover, inhibiting PLA2G7 may disrupt the immunosuppressive TME shaped by intratumoral macrophages and promote CD8 T-cell immunity in HCC.

Darapladib, the most advanced Lp-PLA2 inhibitor employed in this study, has undergone phase III clinical trials aimed at mitigating atherosclerosis by targeting vascular inflammation. However, certain clinical trials have not conclusively demonstrated its significant efficacy in reducing cardiovascular events, leading to limitations in its clinical adoption.[26] Nevertheless, the multifaceted mechanisms of action exhibited by darapladib have sparked researchers' interest beyond the realm of cardiovascular health. A growing body of research has revealed potential connections between darapladib and conditions such as diabetic macular edema[27] and Alzheimer's disease.[28] Recent studies have also highlighted the potential of darapladib as an antitumor agent. For instance, Wang *et al* demonstrated its efficacy as an anti-glioma compound by inducing mitochondrial membrane depolarization and cellular apoptosis.[29] Oh *et al* revealed that darapladib may synergize with ferroptosis inducers, inhibiting gastric tumor growth.[30] However, these findings emanated from either in vitro experiments or studies employing immune-deficient nude mice, overlooking the immunological components within the TME. In this study, we demonstrated that inhibiting PLA2G7 with darapladib could sensitize HCC to ICB therapy by reprogramming TAMs toward an immunostimulatory phenotype, revealing a novel therapeutic strategy that harnesses the immunomodulatory properties of darapladib for synergistic approaches in cancer treatment.

The dichotomy observed, where darapladib serves as an anti-inflammatory drug in atherosclerosis but promotes immunity in HCC, may be attributed to the intricate biological function of Lp-PLA2 across various pathological conditions.[9] Previous studies proposed that Lp-PLA2 primarily hydrolyzes platelet-activating factor (PAF) and oxidized low-density lipoprotein (oxLDL) into two bioactive products, lysophosphatidylcholine (lysoPC) and oxidized non-esterified fatty acids.[31] LysoPC constitute the major contributors to Lp-PLA2-derived pro-inflammatory effects in atherosclerosis.[32] Conversely, in other pathological conditions where PAF and its analogs, along with truncated oxLDL, potentially induce inflammatory responses, Lp-PLA2 may manifest anti-inflammatory effects.[33] Additionally, research suggested that the binding of Lp-PLA2 to various lipoproteins likely elicits distinct physiological responses.[9 34] In our study, we ascertained that inhibiting PLA2G7 with darapladib activated both the NF-κB and MAPK pathways in TAMs. Blocking NF-κB pathway could counteract the phenotypic changes induced by darapladib in TAMs, while MAPK pathway blockage did not. These data suggest that PLA2G7 primarily promotes macrophage phenotypic transition by modulating the NF-κB pathway. Several studies have provided evidence that bioactive lipid metabolites generated by Lp-PLA2 possess the ability to impede the activity of NF-κB pathway under specific contextual settings.[35–37] However, the intricate nuances of these mechanisms demand further elucidation through subsequent research undertakings.

CONCLUSION

In summary, our study revealed that the PLA2G7^{high} macrophage represents a highly immunosuppressive subset within HCC TME and hinders CD8 T-cell activation. Darapladib, an inhibitor of PLA2G7, demonstrated the potential to diminish HCC tumor burden and overcome resistance to anti-PD-1 treatment in HCC. These discoveries emphasize the previously overlooked role of PLA2G7 as a potent regulator of tumor immunity and a promising adjunctive target to enhance immunotherapy efficacy.

Author affiliations
[1]Department of Gastroenterology and Hepatology, Zhongshan Hospital, Fudan University, Shanghai, China
[2]Shanghai Institute of Liver Disease, Shanghai, China
[3]Shanghai Medical College of Fudan University, Shanghai, China

Contributors FZ, WL, and FM designed and performed experiments, analyzed data, and wrote the manuscript. QJ, WT, ZL, and XL provided patient tissue samples and analyzed clinical data. FZ, WL, and FM were responsible for the animal model establishment. SZ, QJ and WT provided technical and material support. SZ, ZL, XL, and RX provided scientific input and critical constructs. RX, SZ, and LD supervised the entire project and revised the manuscript. SZ and LD are responsible for the overall content as the guarantors.

Funding This study was supported by grants from the National Natural Science Foundation of China (82270135, 82273027, and 81972234), the Natural Science Foundation of Shanghai (21ZR1408900), and the Outstanding Youth Fund of Natural Science Foundation of Anhui Province (2308085J27).

Competing interests None declared.

Patient consent for publication Not applicable.

Ethics approval The study was reviewed and approved by the Ethics Committee of Zhongshan Hospital, Fudan University, Shanghai, China (No. B2022-554R). Participants gave informed consent to participate in the study before taking part.

Provenance and peer review Not commissioned; externally peer reviewed.

Data availability statement Data are available upon reasonable request. Data are available from The Cancer Genome Atlas (http://cancergenome.nih.gov/), and series GSE14520 and GSE140228 in the GEO (Gene Expression Omnibus) website (https://www.ncbi.nlm.nih.gov/geo/). Other data analyzed in this study are available upon reasonable request.

ORCID iD

Ling Dong http://orcid.org/0000-0001-5995-7673

REFERENCES

1 Sung H, Ferlay J, Siegel RL, *et al*. Global cancer Statistics 2020: GLOBOCAN estimates of incidence and mortality worldwide for 36 cancers in 185 countries. *CA Cancer J Clin* 2021;71:209–49.
2 Llovet JM, Kelley RK, Villanueva A, *et al*. Hepatocellular carcinoma. *Nat Rev Dis Primers* 2021;7:6.
3 Morad G, Helmink BA, Sharma P, *et al*. Hallmarks of response, resistance, and toxicity to immune Checkpoint blockade. *Cell* 2021;184:5309–37.
4 El-Khoueiry AB, Sangro B, Yau T, *et al*. Nivolumab in patients with advanced hepatocellular carcinoma (Checkmate 040): an open-label, non-comparative, phase 1/2 dose escalation and expansion trial. *Lancet* 2017;389:2492–502.
5 Kelley RK, Rimassa L, Cheng A-L, *et al*. Nivolumab versus sorafenib in advanced hepatocellular carcinoma (Checkmate 459): a randomised, Multicentre, open-label, phase 3 trial. *Lancet Oncol* 2022;23:995–1008.
6 Tian Z, Hou X, Liu W, *et al*. Macrophages and hepatocellular carcinoma. *Cell Biosci* 2019;9:79.
7 Cheng K, Cai N, Zhu J, *et al*. Tumor-associated Macrophages in liver cancer: from mechanisms to therapy. *Cancer Commun (Lond)* 2022;42:1112–40.
8 Nakamura K, Smyth MJ. Myeloid immunosuppression and immune checkpoints in the tumor Microenvironment. *Cell Mol Immunol* 2020;17:1–12.
9 Huang F, Wang K, Shen J. Lipoprotein-associated Phospholipase A2: the story continues. *Med Res Rev* 2020;40:79–134.
10 Casas JP, Ninio E, Panayiotou A, *et al*. Pla2G7 genotype, lipoprotein-associated Phospholipase A2 activity, and coronary heart disease risk in 10 494 cases and 15 624 controls of European ancestry. *Circulation* 2010;121:2284–93.
11 Canning P, Kenny B-A, Prise V, *et al*. Lipoprotein-associated Phospholipase A2 (LP-Pla2) as a therapeutic target to prevent retinal Vasopermeability during diabetes. *Proc Natl Acad Sci U S A* 2016;113:7213–8.
12 Li Q, Feng C, Li L, *et al*. Lipid receptor G2A-mediated signal pathway plays a critical role in inflammatory response by promoting classical macrophage activation. *J Immunol* 2021;206:2338–52.
13 Alinezhad S, Väänänen R-M, Mattsson J, *et al*. Validation of novel biomarkers for prostate cancer progression by the combination of Bioinformatics. *PLoS One* 2016;11:e0158255.
14 Morigny P, Kaltenecker D, Zuber J, *et al*. Association of circulating Pla2G7 levels with cancer Cachexia and assessment of Darapladib as a therapy. *J Cachexia Sarcopenia Muscle* 2021;12:1333–51.
15 Zheng W, Lin Q, Issah MA, *et al*. Identification of Pla2G7 as a novel biomarker of diffuse large B cell lymphoma. *BMC Cancer* 2021;21.
16 Saenger Y, Magidson J, Liaw B, *et al*. Blood mRNA expression profiling predicts survival in patients treated with Tremelimumab. *Clin Cancer Res* 2014;20:3310–8.
17 Lehtinen L, Vainio P, Wikman H, *et al*. Pla2G7 Associates with hormone receptor Negativity in clinical breast cancer samples and regulates epithelial-Mesenchymal transition in cultured breast cancer cells. *J Pathol Clin Res* 2017;3:123–38.
18 Lencioni R, Llovet JM. Modified RECIST (mRECIST) assessment for hepatocellular carcinoma. *Semin Liver Dis* 2010;30:52–60.
19 Sun Y, Wu L, Zhong Y, *et al*. Single-cell landscape of the Ecosystem in early-relapse hepatocellular carcinoma. *Cell* 2021;184:404–21.
20 Zhang Q, He Y, Luo N, *et al*. Landscape and Dynamics of single immune cells in hepatocellular carcinoma. *Cell* 2019;179:829–45.
21 Hao Y, Hao S, Andersen-Nissen E, *et al*. Integrated analysis of Multimodal single-cell data. *Cell* 2021;184:3573–3587.
22 Zhang C, Li J, Cheng Y, *et al*. Single-cell RNA sequencing reveals Intrahepatic and peripheral immune characteristics related to disease phases in HBV-infected patients. *Gut* 2023;72:153–67.
23 Li Y, Tian B, Yang J, *et al*. Stepwise metastatic human hepatocellular carcinoma cell model system with multiple metastatic potentials established through consecutive in vivo selection and studies on metastatic characteristics. *J Cancer Res Clin Oncol* 2004;130.
24 Li H, Xiao Y, Li Q, *et al*. The allergy mediator histamine confers resistance to Immunotherapy in cancer patients via activation of the macrophage histamine receptor H1. *Cancer Cell* 2022;40:36–52.
25 Philip M, Schietinger A. Cd8(+) T cell differentiation and dysfunction in cancer. *Nat Rev Immunol* 2022;22:209–23.
26 Mullard A. GSK's Darapladib failures dim hopes for anti-inflammatory heart drugs. *Nat Rev Drug Discov* 2014;13:481–2.
27 Staurenghi G, Ye L, Magee MH, *et al*. Darapladib, a lipoprotein-associated Phospholipase A2 inhibitor, in diabetic macular edema: a 3-month placebo-controlled study. *Ophthalmology* 2015;122:990–6.
28 Acharya NK, Levin EC, Clifford PM, *et al*. Diabetes and hypercholesterolemia increase blood-brain barrier permeability and brain Amyloid deposition: beneficial effects of the Lppla2 inhibitor Darapladib. *J Alzheimers Dis* 2013;35:179–98.
29 Wang Y-J, Chang S-B, Wang C-Y, *et al*. The selective lipoprotein-associated Phospholipase A2 inhibitor Darapladib triggers irreversible actions on glioma cell apoptosis and mitochondrial dysfunction. *Toxicol Appl Pharmacol* 2020;402:115133.
30 Oh M, Jang SY, Lee J-Y, *et al*. The lipoprotein-associated Phospholipase A2 inhibitor Darapladib Sensitises cancer cells to Ferroptosis by remodelling lipid metabolism. *Nat Commun* 2023;14:5728.
31 Dennis EA, Cao J, Hsu YH, *et al*. Phospholipase A2 enzymes: physical structure, biological function, disease implication, chemical inhibition, and therapeutic intervention. *Chem Rev* 2011;111:6130–85.
32 Zalewski A, Macphee C. Role of lipoprotein-associated Phospholipase A2 in Atherosclerosis: biology, epidemiology, and possible therapeutic target. *Arterioscler Thromb Vasc Biol* 2005;25:923–31.
33 Du Y, Yang M, Wei W, *et al*. Macrophage VLDL receptor promotes PAFAH secretion in mother's milk and suppresses systemic inflammation in nursing neonates. *Nat Commun* 2012;3:1008.
34 Tellis CC, Tselepis AD. Pathophysiological role and clinical significance of lipoprotein-associated Phospholipase A_2 (LP-PLA_2) bound to LDL and HDL. *Curr Pharm Des* 2014;20:6256–69.
35 Carneiro AB, Iaciura BMF, Nohara LL, *et al*. Lysophosphatidylcholine triggers Tlr2- and Tlr4-mediated signaling pathways but Counteracts LPS-induced NO synthesis in peritoneal Macrophages by inhibiting NF-ΚB translocation and MAPK/ERK Phosphorylation. *PLoS One* 2013;8:e76233.
36 Maciel E, Neves BM, Martins J, *et al*. Oxidized Phosphatidylserine mitigates LPS-triggered macrophage inflammatory status through modulation of JNK and NF-kB signaling cascades. *Cell Signal* 2019;61:30–8.
37 Chien HY, Lu CS, Chuang KH, *et al*. Attenuation of LPS-induced Cyclooxygenase-2 and inducible NO synthase expression by Lysophosphatidic acid in Macrophages. *Innate Immun* 2015;21:635–46.